

NANOFUIDICS

Modeling of emergent memory and voltage spiking in ionic transport through angstrom-scale slits

Paul Robin, Nikita Kavokine, Lydéric Bocquet*

Recent advances in nanofuidics have enabled the confinement of water down to a single molecular layer. Such monolayer electrolytes show promise in achieving bioinspired functionalities through molecular control of ion transport. However, the understanding of ion dynamics in these systems is still scarce. Here, we develop an analytical theory, backed up by molecular dynamics simulations, that predicts strongly nonlinear effects in ion transport across quasi-two-dimensional slits. We show that under an electric field, ions assemble into elongated clusters, whose slow dynamics result in hysteretic conduction. This phenomenon, known as the memristor effect, can be harnessed to build an elementary neuron. As a proof of concept, we carry out molecular simulations of two nanofuidic slits that reproduce the Hodgkin-Huxley model and observe spontaneous emission of voltage spikes characteristic of neuromorphic activity.

Neurotransmission relies on the harmonious transport of manifold ionic species across the cellular membrane (1, 2). In particular, the nonlinear, history-dependent dynamics of biological ion channels (3) is key to many neuronal processes. Although considerable progress in the design of new nanofuidic devices has been achieved over the past decade (4–10), artificial systems still cannot compete with the ionic machinery of neurons. This points to the need for the invention and design of artificial iontronic devices with advanced functionalities (4). Most notably, an ion-based memristor—short for memory resistor, an electronic device with hysteretic conductance (11, 12)—could serve as an elementary building block for ion-based neuromorphic systems. In the fabrication of nanofuidic systems, a milestone has very recently been reached, as planar confinement of an electrolyte down to a single molecular layer (see Fig. 1, A and B) was demonstrated and investigated experimentally (13–15). Extremely confined systems are promising from a functional point of view (16): Because they are most sensitive to the discrete nature of ions (17, 18), they are prone to exhibiting exotic transport properties (15, 19, 20). Yet, modeling such subnanometric systems requires going beyond the traditional Poisson-Nernst-Planck (PNP) equations (18) because the reduced dimensionality drastically affects the nature of charge interactions and results in qualitative changes in the conduction dynamics (20). Here, we develop a theoretical and numerical framework to study such two-dimensional (2D) systems and show how they can be used to build new iontronic devices inspired by biological neurons.

In bulk electrolytes, ionic transport is essentially linear because the high dielectric constant of water reduces the strength of ionic interactions. Conversely, in 1D geometries (such as in carbon nanotubes), translational degrees of freedom are extremely constrained, limiting correlation times and potential memory effects. Here, we focus on an intermediate geometry: a monolayer of ions, molecularly confined in a subnanometric slit (see Fig. 1). In such strong planar confinement, ions experience not only a reduction in translational freedom but also stronger electrostatic interactions whose nature is intermediate between that of 3D and 2D systems, which we term “2D⁺” interactions.

We first investigate the equilibrium properties of 2D electrolytes. Using all-atom molecular dynamics (MD) simulations, we consider aqueous solutions of various salts—such as NaCl, CaCl₂, and CaSO₄—confined in a narrow slit of tunable spacing $h = 0.7, 1.0$ or 1.4 nm (amounting to one, two, and three water layers, respectively) made of two sheets of graphene or hexagonal boron nitride. Details of the simulations are provided in the supplementary materials. Although these salts are known to be completely dissociated in bulk solutions, we find that in monolayer confinement, they may form tightly bound Bjerrum pairs (21) (see Fig. 1C)—and even triplets, in the case of CaCl₂. Even in two- or three-layer confinement, all salts except NaCl still associate into pairs. This pairing was recently predicted for electrolytes confined in 1D carbon nanotubes (20) and can similarly be explained in the 2D⁺ case in terms of the confinement-induced effective interaction between the ions. Because the water dielectric permittivity ϵ_w is much larger than that of the confining medium, the electric field lines created by an ion are forced to remain parallel to the channel walls over a typical length ξ . An exact computation, reported in the supplementary text, yields, in the case of a symmetric electrolyte, the cor-

responding pair-wise interaction potential (see fig. S3):

$$\beta V_{ij}(r) = -\frac{q_i q_j}{T^*} \log \frac{r}{r + \xi} \quad (1)$$

where β is inverse temperature, V_{ij} is the interaction potential between ions i and j , r is the distance between the two ions, $q_{i,j} = \pm 1$ is the charge sign, and $1/T^*$ is a dimensionless coupling constant. We derive the precise expressions of $V(r)$, T^* , and the dielectric length ξ in the supplementary text (see section 3.1), notably in the experimentally relevant case where the dielectric permittivity of confined water is anisotropic (22, 23). In the case of divalent salt in a slit of height $h = 0.7$ nm at room temperature, we typically find $T^* = 0.11$ and $\xi = 14$ nm. The corresponding Bjerrum length ℓ_B , defined by $\beta V(\ell_B) = 1$, is 130 nm, which is much larger than the Bjerrum length in bulk water ($\ell_B = 0.7$ nm). Therefore, the interaction potential in Eq. 1 is much stronger than its bulk counterpart $V_{\text{bulk}}(r) = e^2/4\pi\epsilon_0\epsilon_w r$; this qualitatively explains the confinement-induced ion pairing. The coupling constant $1/T^*$ is also proportional to Z^2/h , where Z is the valence of ions, explaining why monovalent ions only form pairs in the thinnest slits.

To identify the range of effective temperatures and ionic concentrations in which Bjerrum pairing occurs (Fig. 1D), we performed implicit solvent Brownian dynamics (BD) simulations of a symmetric electrolyte interacting with the derived potential in Eq. 1. At a short distance ($r \ll \xi$), our interaction potential is logarithmic and resembles a 2D Coulomb potential. The pairing transition in our monolayer electrolyte is therefore almost described by a 2D Coulomb gas model (24, 25) and is analogous to the Kosterlitz-Thouless (KT) topological phase transition (26). However, the analogy is not perfect because the interaction potential recovers a bulk $1/r$ behavior at large distances $r \gg \xi$. To account for these observations, we use a mean-field approach inspired by Fuoss's theory of bulk electrolytes (27), in which ion pairs are incorporated as a separate species. We are able to determine analytically the pairing transition temperature, both in the ideal 2D and our 2D⁺ setting (Fig. 1D), as detailed in the supplementary text, section 3. Our analytical computation reproduces quantitatively the BD simulations, and the ideal 2D description turns out to be valid for all but the lowest salt concentrations. The ion pairing quasi-KT phase transition appears as a specific feature of the monolayer electrolyte. In 1D confinement, there can be no phase transition (20), and in three dimensions, the ion-ion interactions are usually not strong enough for pairing to occur at room temperature (24). By contrast, our model predicts a transition temperature $T = 350$ K for divalent salts like CaSO₄ in slits with $h = 1.4$ nm or for CaCl₂ with $h = 0.7$ nm.

Laboratoire de Physique de l'École Normale Supérieure, ENS, Université PSL, CNRS, Sorbonne Université, Université de Paris, F-75005 Paris, France.

*Corresponding author. Email: lyderic.bocquet@ens.fr

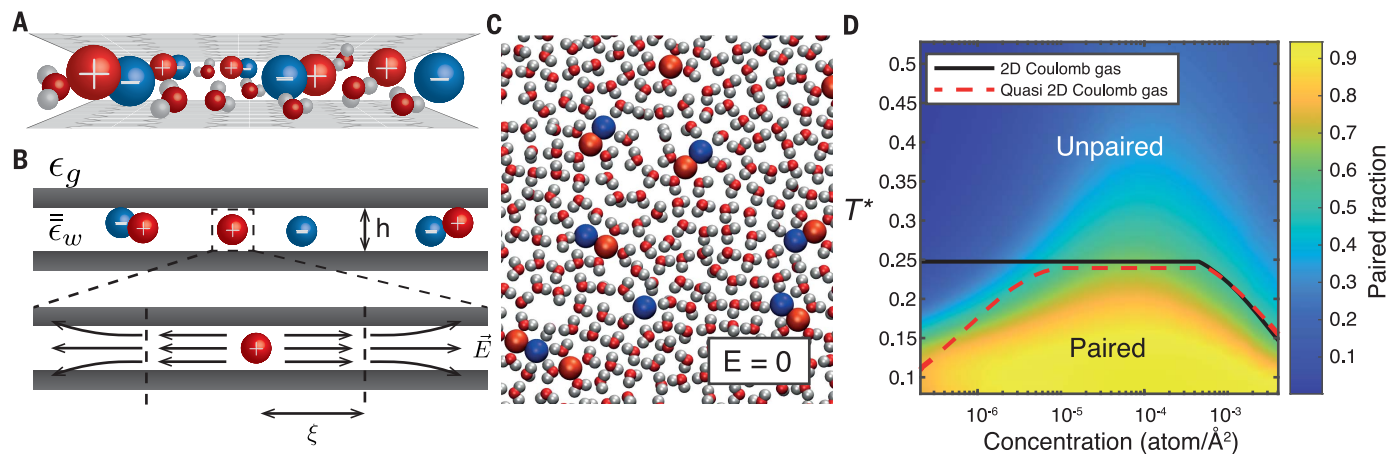
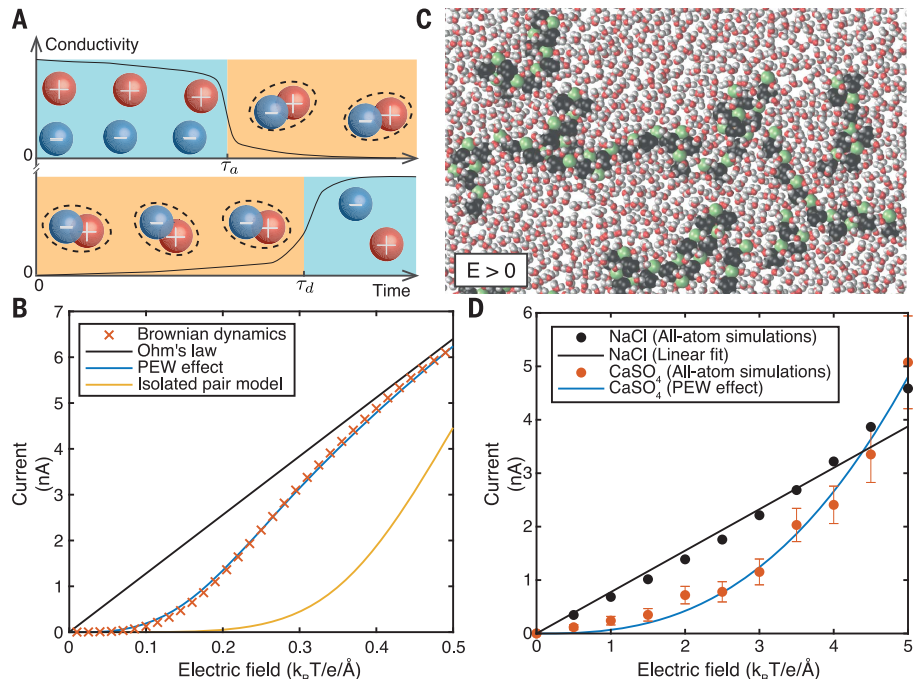


Fig. 1. Simulation and modelization of a 2D electrolyte. (A) Sketch of a 2D electrolyte. Red, sodium ions; blue, chloride ions; red and silver, water molecules. (B) Quasi-2D Coulomb gas model, with $2D^+$ Coulomb interactions given by Eq. 1. The electric field is confined in the channel over a length ξ owing to dielectric contrast between water and graphite. The vertical dashed lines indicate the shift from quasi-2D to 3D electrostatic interactions. ϵ_g , graphite dielectric permittivity; ϵ_w , water dielectric permittivity. (C) Typical configuration of a monolayer electrolyte as observed in

all-atom MD simulations. Sodium ions (in red) and chloride ions (in blue) form tightly bound Bjerrum pairs at room temperature in slits of height $h = 0.7$ nm. (D) Phase diagram of a 2D electrolyte, obtained from Brownian dynamics simulations. At reduced temperature $T^* = 0.25$, the system undergoes a pairing phase transition, analogous to the KT transition. The solid black and dashed red curves correspond to the mean-field prediction for the transition line for an exactly 2D ($\xi = \infty$) or $2D^+$ (finite ξ) Coulomb gas, respectively (see supplementary text).

Fig. 2. Analytical theory of the PEW effect. (A) Schematic representation of Onsager's Wien effect for an isolated ion pair: Free ions have a lifetime of order τ_a during which they contribute to conduction before assembling into pairs (top). Pairs typically break up after a time τ_d and do not take part in conduction (bottom). (B) I-V characteristic of a generic divalent salt. Taking into account the formation of polyelectrolytes substantially improves the agreement with simulations (blue line, see Eqs. 6 and 7) compared with the IP model (yellow line, see Eq. 4) for an ionic concentration $p = 10^{-3}$ atom/nm². (C) Under a constant external field, Bjerrum pairs assemble into complex structures: Bjerrum polyelectrolytes are shown here with CaSO₄. Calcium ions are in green, and sulfate ions are in black. (D) I-V characteristic of CaSO₄ in a 1-nm slit, as obtained from all-atom simulations, compared with the power law $I \propto E^a$ of the PEW effect theory, with the predicted exponent $a = a_{\text{PEW}} = 2.6$. NaCl does not form pairs in slits of that height and exhibits a linear response.



Such strong ionic correlations at equilibrium are at the source of highly nonlinear ion transport, illustrated by the current-voltage (I - V) characteristics obtained from MD simulations (Fig. 2, B and D). This nonlinearity is an indicator that conduction proceeds through the breaking of ion pairs. Consistently, a nonlinear response is observed for CaSO₄, which is paired at equilibrium, unlike NaCl, which does not form pairs in the considered conditions (Fig. 2D).

This type of ion transport is known as the second Wien effect, as famously pioneered

by Onsager (28, 29). We accordingly develop a theory for the Wien effect in the $2D^+$ geometry. We consider a chemical equilibrium between pairs and “free” ions of the form $\text{NaCl} \rightleftharpoons \text{Na}^+ + \text{Cl}^-$ (see Fig. 2A). Assuming that pairs dissociate with a time scale τ_d and free ions assemble into pairs with a time scale τ_a , we obtain an evolution equation for the fraction n_f of free ions not engaged in a pair:

$$\dot{n}_f = \frac{1 - n_f}{\tau_d} - \frac{n_f^2}{\tau_a} \quad (2)$$

Although computing the dependence of τ_d with parameters is usually a mathematical challenge, we were able to reduce it to a self-similar problem in the particular case of $2D^+$ confined electrolytes (see supplementary text, section 3) yielding:

$$\tau_a = \frac{T^*}{4\pi D p} \quad (3)$$

$$\tau_d = \frac{r_0^2}{2D} \left(\frac{l_E}{r_0} \right)^{1/T^*} \quad (4)$$

where the length scale $l_E = k_B T / ZeE$ describes

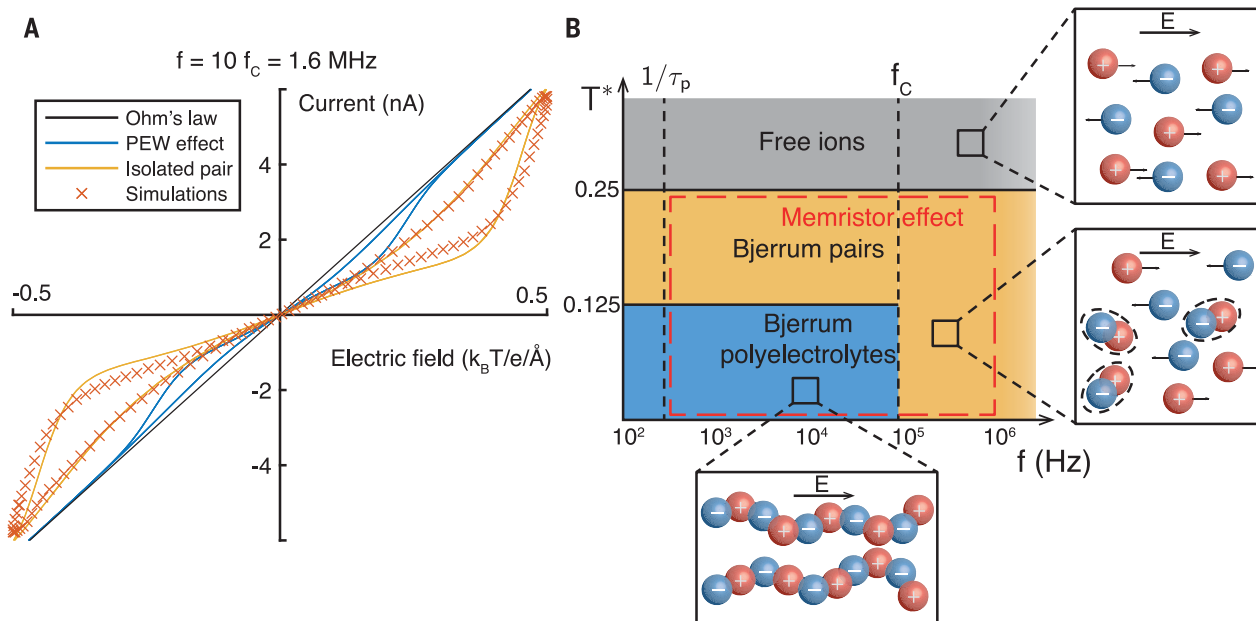


Fig. 3. Time-dependent regime and memristor effect. (A) “Pinched” I - V characteristic at high frequency (here, $f = 10f_C = 1.6 \text{ MHz}$ and $T^* = 0.11$), typical of memristive devices. Here, the IP model (yellow line, Eqs. 2 and 4) provides a better prediction than the PEW effect model (blue line, Eqs. 2 and 6), showing that Bjerrum polyelectrolytes are unstable at

high frequency. (B) Temperature-frequency diagram summarizing the existence domains of Bjerrum pairs and polyelectrolytes for a generic salt with $r_0 = 1 \text{ \AA}$, $D = 10^{-9} \text{ m}^2/\text{s}$, and ionic concentration $\rho \sim 10^{-3} \text{ atom}/\text{nm}^3$. Orders of magnitude for other values of parameters are obtained by noticing that the natural scale for frequencies is D/r_0^2 .

the strength of the external field with respect to thermal fluctuations, k_B is the Boltzmann constant, E is the electric field, D is the diffusion coefficient, ρ is the ionic concentration, and r_0 is the radius of considered ions. Because this model considers ion pairs as independent, noninteracting particles, we refer to it as the isolated pair (IP) model. When the steady state is reached, Eq. 2 can be solved, and the ionic current reads

$$I = N \frac{2ZeD}{k_B TL} E \frac{\tau_a}{2\tau_d} \left(\sqrt{1 + \frac{2\tau_d}{\tau_a}} - 1 \right) \underset{E \rightarrow 0}{\propto} E^{a_{\text{IP}}(T^*)} \quad (5)$$

where N is the number of ions, L is the channel’s length, and $a_{\text{IP}}(T^*) = 1 + 1/2T^*$ is the I - V curve exponent at low applied voltage. However, this prediction fails to reproduce simulation results, even at very low concentrations (see the solid yellow line in Fig. 2B). The all-atom MD simulations provide some hints to understanding this discrepancy. As shown in Fig. 2C, under an external electric field, ion pairs do not actually break but instead rearrange into gigantic clusters with chemistry-specific size and topology (see fig. S1 and supplementary text, section 2). These clusters, which we term “Bjerrum polyelectrolytes,” lead to a radically new phenomenology.

The formation of macrostructures indicates that ion pairs cannot be treated independently, and thus the Wien effect dynamics is fundamentally different from Onsager’s picture.

Going beyond the IP model essentially amounts to taking into account the effect of Debye screening, characterized by the Debye length $\lambda_D = \sqrt{\frac{T}{\rho n_e}}$. Because under a (low) electric field E the density of the free ions is $n_f \sim \tau_d^{-1/2} \propto l_E^{-1/2T^*}$, $\lambda_D \propto l_E^{1/4T^*}$ sets the size of the screening cloud around a given ion. Yet, two ions are carried away from each other if they are separated by a distance exceeding $l_E/T^* \propto l_E$ in the direction of the field, say x . For sufficiently low temperature (or sufficiently large field), $\lambda_D > l_E$ and the ionic atmosphere becomes anisotropic: It extends over l_E in the direction x and over λ_D in the perpendicular direction y . We show in the supplementary text (see section 3.6) that such an anisotropic screening cloud becomes unstable in the direction y below a critical temperature, explaining the formation of Bjerrum polyelectrolytes. In terms of the dynamics, this amounts to modifying the scaling exponent of the pair dissociation time according to (see supplementary text, section 3.6)

$$\tau_d = \frac{r_0^2}{2D} \left(\frac{l_E}{r_0} \right)^{1/2T^*} \quad (6)$$

As per Eq. 5, this results in a new exponent for the current-versus-voltage scaling:

$$I \underset{E \rightarrow 0}{\propto} E^{a_{\text{PEW}}(T^*)}, \quad a_{\text{PEW}}(T^*) = 1 + 1/4T^* \quad (7)$$

We term this new mechanism the polyelectrolytic Wien (PEW) effect, because conduction

actually occurs inside the Bjerrum polyelectrolytes. In Fig. 2B, we show that the PEW prediction is in quantitative agreement with BD simulation results, in contrast to the IP model. We also compare it to results from all-atom simulations for CaSO_4 in Fig. 2D to demonstrate its robustness: The dynamics of the ionic assemblies is independent of the chemical nature of the salt and the confining medium or of simulation details (see fig. S2). Their formation is a direct consequence of 2D confinement.

The subtle nonlinear transport phenomena unveiled above set the stage for the memristor effect. The fraction of ions that is part of a Bjerrum polyelectrolyte structure is expected to behave as an internal variable, keeping memory of the voltage history. More formally, Eqs. 2 and 5 can be recast in a more transparent form, introducing the voltage U :

$$I = G(n_f) \times U \quad (8)$$

$$\frac{\partial}{\partial t} n_f = f(n_f, U) \quad (9)$$

The fraction of conducting ions, n_f , appears here as an internal state variable that depends on the system’s history. Furthermore, from the previous analysis, the relevant time scale governing the system’s dynamics— τ_a —is much longer than usual molecular time scales, typically with $\tau_a \sim 1 \mu\text{s}$. This points to potential memory effects in the system. Altogether, Eqs. 8 and 9 formally define a voltage-controlled

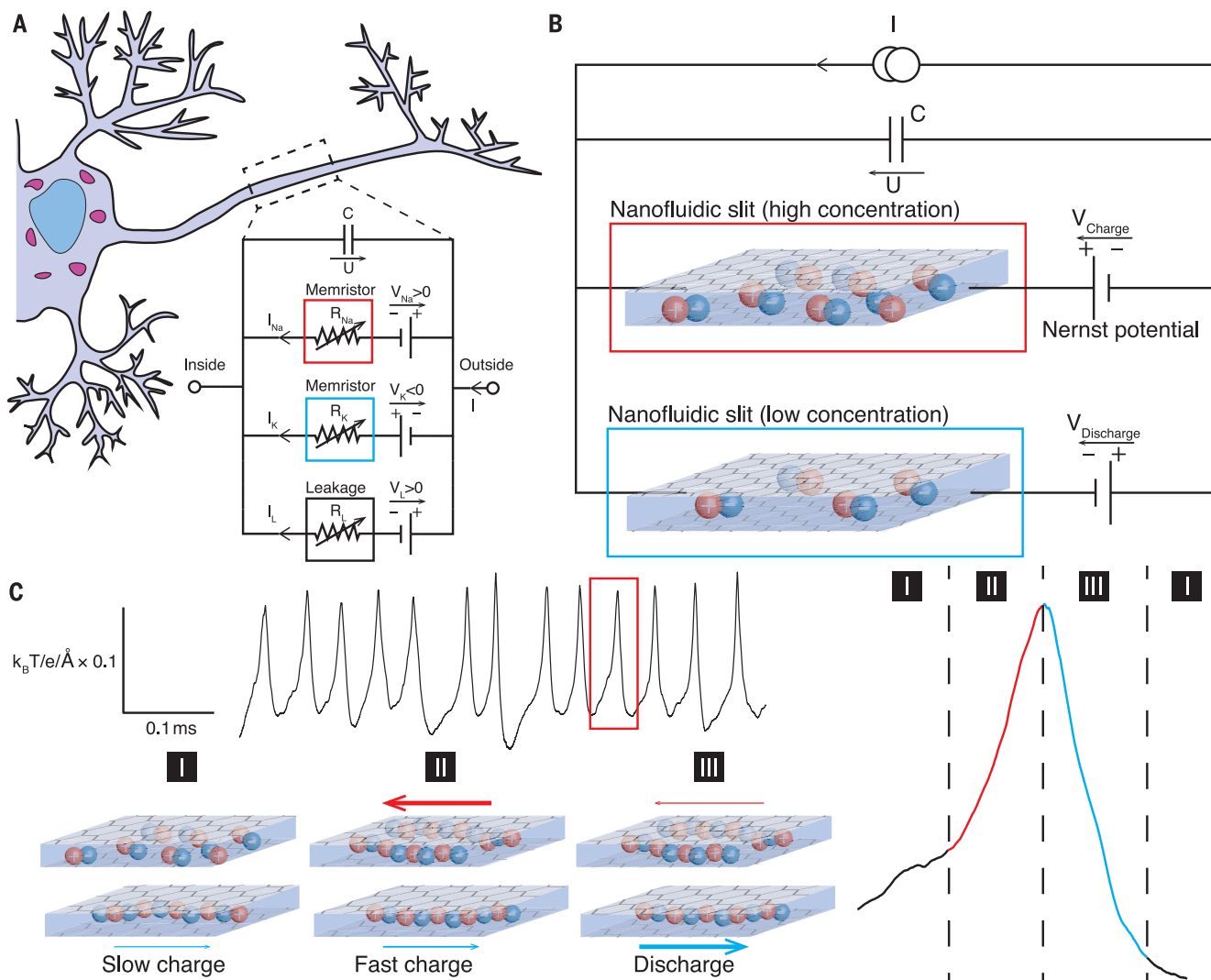


Fig. 4. Building an artificial Hodgkin-Huxley neuron from 2D ionic memristors.

(A) Electronic representation of the Hodgkin-Huxley model, adapted from (3). I_{Na} , R_{Na} , and V_{Na} ; I_K , R_K , and V_K ; and I_L , R_L , and V_L are the current, resistance, and Nernst potential of sodium, potassium, and other species, respectively. (B) Prototype ionic machine implemented in BD simulations, exhibiting primitive neuronal behavior. Two slits with different ionic concentrations are simulated

over long time scales ($t \sim 1$ ms). Each slit is connected to a pair of reservoirs, imposing a given Nernst potential on the slit, as in the original computation by Hodgkin and Huxley. (C) Spontaneous voltage spikes emitted by the prototype ionic machine and qualitative explanation for the observed spiking effect. The right panel shows different phases of a single spike, corresponding to the red rectangle on the left. Black line, quiescent neuron; red line, spike initiation; blue line, discharge.

memristor, an electronic device whose resistance depends on its past (II, I2).

A further proof and hallmark of the memristor behavior is shown in Fig. 3A, because the $I-V$ characteristic under alternating voltage takes the form of a pinched loop for frequencies larger than a threshold f_p . The time scale $\tau_p = 1/f_p$ is found to decrease with ionic concentration ρ , and we interpret it as a formation time scale of Bjerrum polyelectrolyte. Qualitatively, because conduction occurs through the slow formation of macrostructures, the system cannot adapt to the instantaneous value of the electric field. Once the polyelectrolytes form, they contribute to conduction even if the field is turned off, before eventually dissolving. We

compare the BD simulation results with our Wien effect theory to get insight into the underlying physics of the memristor behavior. We find that below a threshold frequency f_C (here $f_C = 160$ kHz), the simulated $I-V$ curves are well reproduced by the PEW model, whereas for $f > f_C$, quantitative agreement is observed with the IP model (see Fig. 3B and fig. S4). This is consistent with the observation that at high frequencies, polyelectrolytes do not have time to form and conduction proceeds through the breaking of individual pairs. The threshold frequency $f_C = 160$ kHz is found to be independent of concentration and is therefore related to the dynamics of individual Bjerrum polyelectrolytes.

Although in our simulations the frequency of the alternating field is high owing to numerical constraints, our model predicts that it should also be relevant in a realistic experimental setting. We show in the supplementary text that a memristor effect could be observed at experimentally relevant frequencies $f \sim 100$ Hz and voltages $U \sim 0.1$ V (see fig. S5). The memory effect is driven by Bjerrum pairs and polyelectrolytes, which form in all salts regardless of their chemical nature. Therefore, the memristor effect, described by Eqs. 8 and 9, is a universal property of 2D electrolytes. We also find that optimal conditions correspond to a divalent salt with a slit height close to 1 nm, with other parameters such as the chemical structure

of ions or of the confining material playing little role.

Memristors are the electric equivalents of voltage-gated ion channels. As such, they may serve as components of a primitive neuron, as first pointed out by Hodgkin and Huxley (3) (Fig. 4A). Hence, it is expected that assembling several nanofluidic memristors would allow neuromorphic behavior to be mimicked. To demonstrate this possibility, we perform parallel BD simulations of two monolayer electrolytes confined in two separate molecular channels (see Fig. 4B). For both electrolytes, the simulation yields the instantaneous relation between the applied voltage and resulting ionic current. A numeric circuitry is designed around the simulated molecular systems to reproduce the Hodgkin-Huxley model (see Fig. 4A). It includes a capacitor and opposite sign potentials applied on each channel that account for the Nernst potentials. The electronic circuit and the molecular channels are then simulated together, with the capacitor applying a voltage drop across the channels. Further details of the simulations are given in the supplementary text. We observe spontaneous voltage spikes at a frequency around 10 kHz (Fig. 4B). These spikes are the hallmark of neuromorphic behavior, obtained here from the sole properties of monolayer electrolytes.

The qualitative mechanism behind the generation of the spikes can be understood as follows: Because the two electrolytes are subject to (Nernst) potentials of opposite signs, they conduct current in opposite directions, but they are gated by the same voltage U . When U is small, only the discharging memristor is conducting, so that the capacitor receives a current $I_C < I$ and slowly charges. When U reaches a threshold value, the charging memristor starts conducting and the capacitor receives $I_C \gg I$, causing the voltage to spike up to $U \sim V_{\text{charge}}$. Then, the discharging memristor takes over: The capacitor receives a strongly negative current, and its voltage is lowered back to 0, at which point the process can start again (see Fig. 4C). This whole process is analogous to voltage spiking

in biological neurons caused by the successive opening and closing of ion channels (sodium and potassium channels in the case of the Hodgkin-Huxley model of the giant squid axon). The observed working frequency of a few kilohertz is, considering the set of parameters used in simulations, just above the threshold frequency for the memristor effect, which is therefore crucial for observing the neuromorphic behavior.

The proper design of an experimentally accessible nanofluidic channel enables reproduction of the physical processes that occur in an elementary neuron, capable of emitting voltage spike trains. This result builds on the far-from-equilibrium transport properties of electrolytes in molecularly confined nanochannels, whose conductivity highlights a memristor effect. Our findings are supported by molecular simulations, combined with an extensive theoretical framework for the nonequilibrium transport, which generalizes Onsager's description of the Wien effect. These properties build on the 2D⁺ nature of such channels, where the magnitude of ionic correlations is intermediate between bulk and 1D systems. This theoretical prototyping is the first step toward an experimental demonstration of the ionic memristor, and exploration of memory phenomena in nanofluidic systems in general. The complex interplay between water, surfaces, and ions at the nanoscale gives rise to larger spatial structures—here, polyelectrolytes—which entail the emergence of slow dynamics and long memory times.

REFERENCES AND NOTES

- B. Hille, *Biophys. J.* **22**, 283–294 (1978).
- W. Gerstner, W. M. Kistler, *Spiking Neuron Models: Single Neurons, Populations, Plasticity* (Cambridge Univ. Press, 2002).
- A. L. Hodgkin, A. F. Huxley, *J. Physiol.* **117**, 500–544 (1952).
- L. Bocquet, *Nat. Mater.* **19**, 254–256 (2020).
- S. Garaj et al., *Nature* **467**, 190–193 (2010).
- C. Y. Lee, W. Choi, J.-H. Han, M. S. Strano, *Science* **329**, 1320–1324 (2010).
- K. Celebi et al., *Science* **344**, 289–292 (2014).
- J. Feng et al., *Nature* **536**, 197–200 (2016).
- E. Secchi et al., *Nature* **537**, 210–213 (2016).
- R. H. Tunuguntla et al., *Science* **357**, 792–796 (2017).
- L. Chua, *IEEE Trans. Circuit Theory* **18**, 507–519 (1971).
- D. B. Strukov, G. S. Snider, D. R. Stewart, R. S. Williams, *Nature* **453**, 80–83 (2008).
- B. Radha et al., *Nature* **538**, 222–225 (2016).
- A. Esfandiar et al., *Science* **358**, 511–513 (2017).
- T. Mouterde et al., *Nature* **567**, 87–90 (2019).
- S. Faucher et al., *J. Phys. Chem. C* **123**, 21309–21326 (2019).
- W. Sparreboom, A. van den Berg, J. C. T. Eijkel, *New J. Phys.* **12**, 015004 (2010).
- N. Kavokine, R. R. Netz, L. Bocquet, *Annu. Rev. Fluid Mech.* **53**, 377–410 (2021).
- A. Marcotte, T. Mouterde, A. Niguès, A. Siria, L. Bocquet, *Nat. Mater.* **19**, 1057–1061 (2020).
- N. Kavokine, S. Marbach, A. Siria, L. Bocquet, *Nat. Nanotechnol.* **14**, 573–578 (2019).
- N. Bjerrum, *Untersuchungen über Ionenassoziation* (Dansk Vid. Selskab, Matematisk-fysiske meddelelser, København: A. F. Høst, 1926), pp. 1–48.
- A. Schlaich, E. W. Knapp, R. R. Netz, *Phys. Rev. Lett.* **117**, 048001 (2016).
- L. Fumagalli et al., *Science* **360**, 1339–1342 (2018).
- Y. Levin, *Rep. Prog. Phys.* **65**, 1577–1632 (2002).
- P. Minnhagen, *Rev. Mod. Phys.* **59**, 1001–1066 (1987).
- J. M. Kosterlitz, D. J. Thouless, *J. Phys. C Solid State Phys.* **6**, 1181–1203 (1973).
- R. M. Fuoss, *J. Am. Chem. Soc.* **81**, 2659–2662 (1959).
- L. Onsager, *J. Chem. Phys.* **2**, 599–615 (1934).
- V. Kaiser, thesis, Ecole Normale Supérieure de Lyon (2014).
- P. Robin, N. Kavokine, L. Bocquet, Molecular dynamics code for: Modeling of emergent memory and voltage spiking in ionic transport through angstrom-scale slits. Zenodo (2021); <https://doi.org/10.5281/zenodo.4841109>.

ACKNOWLEDGMENTS

We thank H. Yoshida for help and discussions on molecular dynamics. **Funding:** L.B. acknowledges funding from the EU H2020 Framework Programme/ERC Advanced Grant agreement number 78591-Shadoks and ANR project Neptune. This work has received the support of “Institut Pierre-Gilles de Gennes” program ANR-10-IDEX-0001-02 PSL and ANR-10-LABX-31. This work was granted access to the HPC resources of CINES under the allocation A0090710395 made by GENCI. **Author contributions:** L.B. conceived the project. P.R. carried out the theoretical analysis and the molecular dynamics simulations, with inputs from all authors. All authors discussed the results, co-wrote the article, and reviewed the final manuscript. **Competing interests:** The authors declare no competing interests. **Data and materials availability:** All data are in the main text or supplementary materials. The molecular dynamics codes that support the plots within this paper and other findings of this study are archived on Zenodo (30).

SUPPLEMENTARY MATERIALS

science.sciencemag.org/content/373/6555/687/suppl/DC1
Supplementary Text
Figs. S1 to S5
Table S1
References (31–47)

19 November 2020; accepted 11 June 2021

10.1126/science.abf7923

Modeling of emergent memory and voltage spiking in ionic transport through angstrom-scale slits

Paul Robin, Nikita Kavokine, and Lydric Bocquet

Science, 373 (6555), .
DOI: 10.1126/science.abf7923

Confined flow effects

Most memory resistor (“memristor”) systems use electrons as the charge carrier but it may also be possible to use ionic carriers, similar to the way that neurons work. Robin *et al.* studied an aqueous electrolyte confined into a pseudo two-dimensional gap between two graphite layers (see the Perspective by Hou and Hou). The authors observed a current–voltage relation that exhibits hysteresis, and the conductance depends on the history of the system, also known as the memresistor effect. Using simulations of their system, they can model the emission of voltage spikes characteristic of neuromorphic activity. —MSL

View the article online

<https://www.science.org/doi/10.1126/science.abf7923>

Permissions

<https://www.science.org/help/reprints-and-permissions>